14th International Symposium on Turbulence and Shear Flow Phenomena (TSFP14)
Heidelberg, Germany, July 28–31, 2026

FORCING LENGTH-SCALE EFFECTS ON THE TURBULENT TRANSITION IN INTERNALLY HEATED AND INTERNALLY COOLED CONVECTION

Marten Klein
Numerical Fluid and Gas Dynamics
BTU Cottbus-Senftenberg
Siemens-Halske-Ring 15a,
03046 Cottbus, Germany
marten.klein@b-tu.de

Heiko Schmidt
Numerical Fluid and Gas Dynamics
BTU Cottbus-Senftenberg
Siemens-Halske-Ring 15a,
03046 Cottbus, Germany
heiko.schmidt@b-tu.de

Alan R. Kerstein
Consultant, Stochastic Science
72 Lomitas Road,
Danville, CA 94526, U.S.A.
alan.kerstein@gmail.com

ABSTRACT

The effect of the forcing length scale on the scaling of the heat transport in radiatively driven, vertical convection is numerically investigated using stochastic one-dimensional turbulence as standalone tool. Radiative forcing is modeled by an internal heat source parameterized by a vertical exponential heating-rate profile together with uniform bulk cooling to enforce an exact energy balance. Both the forcing length scale and the total heat flux are prescribed and varied across several orders of magnitude. It is shown here that the stochastic model is able to predict the turbulent transition between the diffusion and mixing-length dominated convection regimes, reproducing and extending established reference results. On this basis it is argued that the transition predicted by the model is a robust physical result as it is accompanied by the degradation of small-scale wall-attached turbulence in a persisting background of bulk turbulence.

INTRODUCTION

Turbulent convective flows are driven by buoyancy forces and occur in numerous applications with temperature inhomogeneities, ranging from microscopic to astrophysical scales (Chillà & Schumacher, 2012). The average heat transported by convective flows is often parameterized by an effective power-law scaling, $Nu \sim Ra^p$, where Nu denotes the Nusselt number, which expresses the total heat transport in units of the purely conductive heat transport, and Ra the Rayleigh number, which is a nondimensional measure of the strength of the forcing due to buoyancy relative to viscous damping. Various scaling relations have been reported in the literature, ranging from $p = 1/3$ (classical regime; Malkus, 1954), to $p = 2/7$ (Shraiman & Siggia, 1990), and $p = 1/2$ (ultimate regime; Kraichnan, 1962; Spiegel, 1963). The variety of observed p values has guided speculation about physical processes in turbulent convection, leading to the derivation of upper bounds and scaling relations associated to them. The Grossmann–Lohse theory (Grossmann & Lohse, 2000) provided the first unifying theory for convection by separating boundary-layer and bulk contributions, which explained the observed scaling regimes in canonical Rayleigh–Bénard convection.

In applications ranging from micrometeorology over geophysical to astrophysical flows, convection is often unbounded and driven locally by internal processes. Sources and sinks can emerge from microphysical processes, like radiation (de Lozar & Mellado, 2015) or condensation/evaporation (Chandrakar *et al.*, 2019), among others. As there are no conducting wall boundaries, it is not guaranteed that results obtained for canonical Rayleigh–Bénard convection are applicable to internally heated convection. Goluskin (2016) has categorized configurations for internally heated convection for which theoretical analysis suggests that the heat transport is in fact constrained by the conductive wall boundaries (Wang *et al.*, 2021; Arslan *et al.*, 2021).

An alternative configuration has been proposed by Lepot *et al.* (2018), who used radiative heating to bypass the conductive heat transport bottleneck. Experiments (Lepot *et al.*, 2018; Bouillaut *et al.*, 2019) and direct numerical simulation (Kazemi *et al.*, 2022; Bouillaut *et al.*, 2022) have provided evidence for turbulent transitions from a classical to an ultimate regime in the accessible moderately turbulent regime.

The main objective of this work is to numerically investigate how the turbulent heat transport is affected by the length scale of internal heat sources for an extended parameter range. This is made feasible by a stochastic one-dimensional modeling approach that offers full-scale vertical resolution at highly reduced cost.

FLOW CONFIGURATION

Figure 1 shows a sketch of the internally heated and internally cooled flow configuration investigated. The case setup is based on the experiment of Lepot *et al.* (2018); Bouillaut *et al.* (2019) and consists of a fluid layer that is vertically bounded by two adiabatic no-slip walls located at $z = 0$ and $z = H$, respectively. The fluid is subject to a constant gravity field $g = -g e_z$, where e_z is the unit vector in vertical (z) direction. Radiative forcing is parameterized by an exponential heating

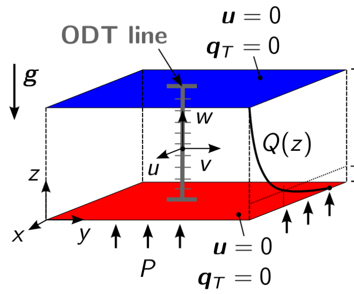

Figure 1. Schematic of the flow configuration.

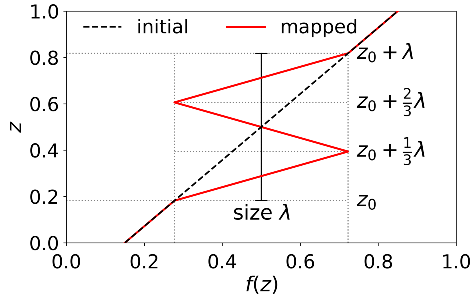

Figure 2. Triplet map $f(z)$ as building block for turbulent advection modeling. The map is parameterized by the size λ and the lower edge location z_0. The midpoint is $z_\mathrm{m} = z_0 + \frac{1}{2}\lambda$.

rate profile, $Q(z) = (P/\ell)\,\exp(-z/\ell)$, where P denotes the radiative power influx from below and ℓ the absorption length represents the length scale of the forcing due to inhomogeneity of the heat source. An exact energy balance is enforced in the numerical setup by a constant uniform cooling rate $-\langle Q\rangle_z$ that compensates the inhomgeneous heating in the volumetric (vertical) average. The effective source-sink forcing is hence given by $Q_\mathrm{tot}(z) = Q(z) - \langle Q\rangle_z$.

MODEL FORMULATION

The so-called one-dimensional turbulence (ODT) model (Kerstein, 1999; Kerstein *et al.*, 2001) is applied to this setup in order to resolve all relevant scales of the turbulent flow along a representative vertical coordinate, here denoted by z (see Fig. 1). Vertical profiles of the temperature and Cartesian velocity components are resolved along a single vertical coordinate using a dynamically adaptive grid (Lignell *et al.*, 2013). The profiles are evolved to together by deterministic and stochastic processes as detailed below.

The ODT governing equations evolve the flow state by modeling the effects of three-dimensional turbulence on a one-dimensional domain ('ODT line' in Fig. 1). The flow state is resolved by vertical profiles of the Cartesian velocity components $u_i(z,t)$, $i = x,y,z$, and the temperature $T(z,t)$. The model equations mimic the momentum and energy equation in a dimensionally reduced form and are given by

$$\frac{\partial u_i}{\partial t} + \mathscr{E}_i = \nu \frac{\partial^2 u_i}{\partial z^2}\,, \tag{1}$$

$$\frac{\partial T}{\partial t} + \mathscr{E}_T = \kappa \frac{\partial^2 T}{\partial z^2} + \frac{Q_\mathrm{tot}}{\rho_0 c_p}\,, \tag{2}$$

where ν denotes the kinematic viscosity, ρ_0 the reference mass density, c_p the specific heat capacity at constant pressure, κ the thermal diffusivity, and Q_tot the internal heat sources and sinks. These equations silently assume the Oberbeck–Boussinesq approximation such that the mass density has a linear dependence on temperature, $\rho(T) = \rho_0\left[1 - \beta\,(T - T_0)\right]$, where β is the thermal expansion coefficient and the subscript 0 denotes the reference values.

The stochastic terms $\mathscr{E}_i$ and $\mathscr{E}_T$ are implemented as a sequence of stochastically sampled mapping events that punctuate the diffusive advancement. A generalized baker's map (triplet map) models the microstructure of instantaneous turbulent mapping events by a conservative vertical displacement of fluid parcels surplus a kernel-based model for pressure–velocity–buoyancy couplings, as detailed in Gonzalez-Juez *et al.* (2013). The rate $\tau^{-1}(\lambda, z_0; t)$ of a selected size-λ turbulent mapping event occurring at location z_0 at time t depends on the specific available energy of the current flow state and is given by

$$\tau^{-1} = C\sqrt{2\lambda^{-2}\left(E_\mathrm{kin} - E_\mathrm{pot} - Z\,E_\mathrm{vp}\right)}\,, \tag{3}$$

where E_kin, E_pot, and E_vp denote the specific kinetic, potential, and viscous penalty energies, respectively. E_pot encodes the equation of state. E_vp is used to effectively suppress mapping events below a viscous cut-off scale that is weakly enforced (Kerstein, 1999; Gonzalez-Juez *et al.*, 2013). The model formulation was previously validated for Rayleigh–Bénard convection systems (Wunsch & Kerstein, 2005; Chandrakar *et al.*, 2019). The free model parameters $C = 60$ and $Z = 220$ have been selected based on the model calibration conducted in Klein & Schmidt (2019) and are kept fixed in this study.

For the configuration in Fig. 1, and the model equations (1) and (2), the flow state is characterized by the Prandtl, Rayleigh, and Nusselt numbers, defined as

$$Pr = \frac{\nu}{\kappa}\,, \quad Ra = \frac{g\,\beta\,\langle\Delta T\rangle\,H^3}{\nu\,\kappa}\,, \quad Nu = \frac{PH}{\rho_0\,c_p\,\kappa\,\langle\Delta T\rangle}\,, \tag{4}$$

where $\Delta T = T|_{z=0} - T|_{z=H/2}$ is a convenient definition of a wall-bulk temperature difference for comparison with Rayleigh–Bénard convection, where $\langle\Delta T\rangle$ denotes a temporal average (Lepot *et al.*, 2018; Bouillaut *et al.*, 2019). Note that the flux-based Rayleigh number, $Ra_P = Ra\,Nu$, together with the nondimensional forcing length scale, ℓ/H, uniquely characterizes the case setup as it is independent of the convective flow state, which enters only through the temperature difference $\langle\Delta T\rangle$. Here, the prescibed nondimensional forcing length scale and flux-based Rayleigh number are varied across $\ell/H \in [3\times10^{-5}, 4\times10^{-1}]$ and $Ra_P \in [10^7, 10^{17}]$, but not always the full Ra_P range is covered for all ℓ/H. The Prandtl number is here fixed at unity.

RESULTS

Flow Profiles

Figure 3 shows instantaneous and time-averaged vertical profiles of the temperature and a horizontal velocity component obtained by ODT for a selected case in the turbulent flow regime, where the mean velocity vanishes. Flow variables are nondimensionalized with the flux-based temperature difference $\Delta T_0 = PH/(\rho_0 c_p \kappa)$ and the flux-based free-fall velocity $U_{\mathrm{f},0} = \sqrt{g\,\beta\,\Delta T_0\,H}$ such that the corresponding free-fall

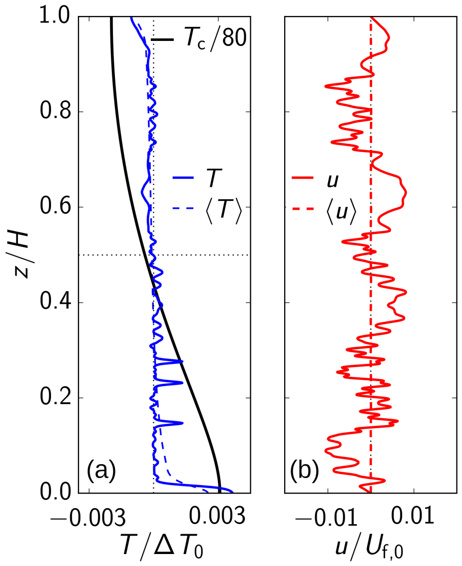

Figure 3. Instantaneous and time-averaged vertical profiles of the temperature T together with a scaled conductive solution T_c, (a), and the corresponding horizontal velocity component $u = u_x$, (b), for turbulent flow. $Ra_P = 10^{10}$ and $\ell/H = 0.096$.

time scale is $t_{f,0} = H/U_{f,0}$. The purely conductive temperature profile $T_c(z)$ is given for orientation, but it is manually scaled to fit in the axes. $T_c(z)$ solves the energy balance exactly under the absence of turbulence. The prescribed adiabatic boundary conditions yield boundary layers that do not contribute to heat transport across domain walls. The magnitude difference of the temperature inhomgeneity between the purely conductive solution $T_c(z)$ and a turbulent solution $T(z,t)$ is due to absence or presence of turbulent mixing, which tends to homogenize the bulk of the fluid layer. The temperature and velocity fluctuations exhibit comparable length scales due to unity Prandtl number.

Nusselt Number

The Rayleigh and Nusselt number definitions collected in (4) serve as basis for the analysis of the convective heat transport, where $\langle \Delta T \rangle$ is obtained from ODT by gathering statistics of the fluctuating temperature $T(0,t)$ at the bottom wall and $T(H/2,t)$ at mid height, simulating long enough to sufficiently sample the state space in order to converge low-order statistical moments. The procedure is analogous to Lepot *et al.* (2018) and Bouillaut *et al.* (2019) with the sole difference that the numerical simulation is statistically stationary whereas the reference experiment is transient.

Following arguments established by Grossmann & Lohse (2000) that have been carried over by Bouillaut *et al.* (2019) to the source-sink convection case, effective scalings of the heat transport regimes can be obtained by separating bulk and boundary-layer contributions. In the current configuration, the prescribed absorption length scale ℓ acts as a control parameter that takes the place of the emerging thermal boundary layer thickness in canonical Rayleigh–Bénard convection. It is therefore reasonable to look for effective scalings that take into account length-scale similarity, suggesting

$$Nu \sim Ra^p \, (\ell/H)^q \qquad \text{for fixed} \quad Pr = 1. \tag{5}$$

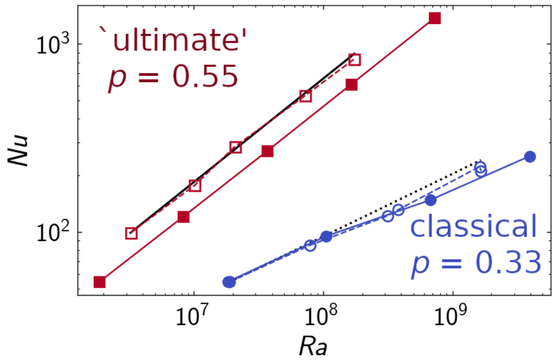

Figure 4. Multipe scalings of the heat transport in source-sink convection. ODT results (filled color symbols) for $Ra_P \in [10^8, 10^{12}]$ at $Pr = 1$ together with reference data from Lepot *et al.* (2018, unfilled black symbols) at $Pr \approx 7$. Selecting $\ell/H = 10^{-4}$ yields classical scaling($p = 0.33$, $\cdots$), whereas $\ell/H = 0.05$ yields 'ultimate' scaling ($p = 0.55$, —).

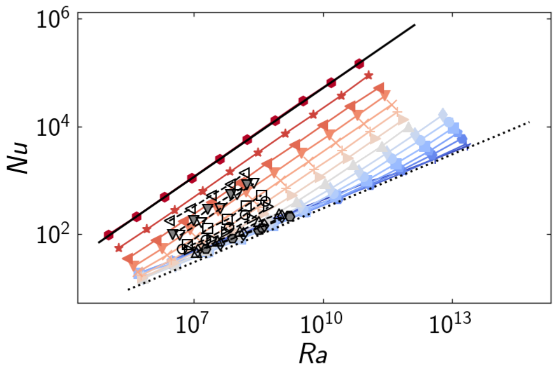

Figure 5. ODT results (filled color symbols) for the heat transport in source-sink convection for an extended parametric range with $Pr = 1$ for $\ell/H \in [3 \times 10^{-5}, 4 \times 10^{-1}]$ (blue-to-red), transitioning from the classical $p = 0.33$ ($\cdots$) to the 'ultimate' $p = 0.55$ (—) regime. Reference data from Bouillaut *et al.* (2019, unfilled black symbols) with $Pr \approx 7$ is given for comparison.

Figure 4 and 5 show multiple scalings of the Nusselt number compatible with equation (5). ODT simulation results for $Pr = 1$ exhibit good qualitative and quantitative agreement with reference experimental results from Lepot *et al.* (2018) and Bouillaut *et al.* (2019) with $Pr \approx 7$, especially for very small absorption lengths, $\ell \ll H$. Here, it is not the objective to reproduce data points exactly, but to assess the scaling relation by varying Ra_P and ℓ/H across several orders of magnitude. Deviations in the prefactor to the Nusselt number manifest themselves as offset in the double-log plots. This discrepancy is indicative of finite Prandtl number and box-size effects. The latter is sensible when the absorption length becomes comparable with the confinement scale, $\ell \lesssim H$. Dashed and solid black lines give the classical $p = 0.33$ (Malkus, 1954) and 'ultimate' $p \simeq 0.55$ (Lepot *et al.*, 2018) scaling, respectively.

Figure 6 shows the same data as Fig. 5, but compensated with power-law scaling of the 'ultimate' regime. For larger absorption length scales, the ODT data appears to be robustly described by $p = 0.55$ (data points colored in dark red), which is in agreement with the first reference experiments from Lepot *et al.* (2018) as shown in Fig. 4. The effect might be transi-

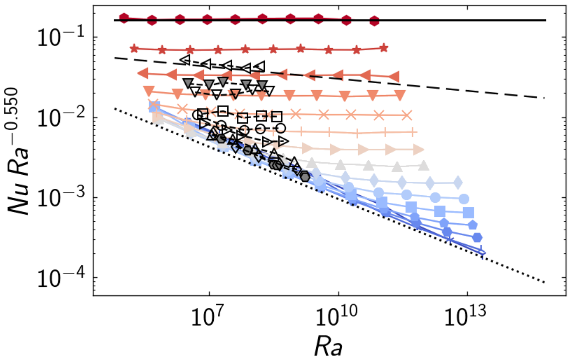

Figure 6. Same data as in Fig. 5, but compensated by the 'ultimate' scaling with $p = 0.55$ (—). The classical scaling with $p = 1/3$ $(\cdots)$ and the conventional ultimate scaling with $p = 1/2$ (– –) are given for orientation. Reference data from Lepot *et al.* (2018, filled gray symbols) and Bouillaut *et al.* (2019, unfilled black symbols) are included for comparison.

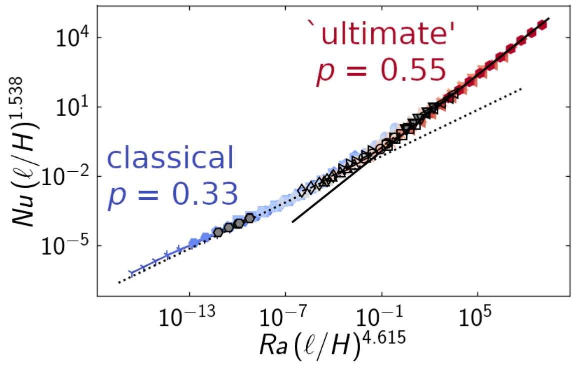

Figure 7. Rescaled reference and ODT data from Fig. 5 after application of the transformation deduced from equation (6).

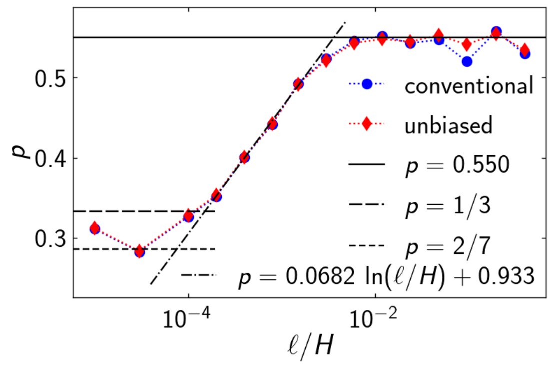

Figure 8. Comparison of effective scaling exponents p across the transition in Fig. 7 obtained with different estimators assuming local effective power-law scalings $Nu \sim Ra^p$. The correlation $p \sim \ln(\ell/H)$ shown in the legend is purely empirical.

tional, caused by truncation of the heating rate profile $Q(z)$ at $z = H$. This will have a sensible effect on the Nusselt number only for fairly large $\ell \simeq O(H)$ since $Q(z)$ will loose its exponential shape only when it is notably truncated since this will lead to a modification of the energy balance across the domain via $Q_{\mathrm{tot}}(z)$. This suggests that the ultimate scaling with $p = 0.55 > 1/2$ could be a transitional effect related to the finite domain size and the modified spatial structure of the source term. This argumentation does not explain the upward bending of blue-colored data sets in the lower right region of Fig. 6 for $Ra \gtrsim 10^{12}$ and $\ell/H \leq 10^{-3}$ which is currently further investigated.

Transition to the Ultimate Regime

Figure 7 shows the extended ODT data set from Fig. 5 for rescaled data Nu/Nu_{X} against Ra/Ra_{X}, where the subscript 'X' indicates a notional transition point. Following Bouillaut *et al.* (2019), the intersection of the classical $(p = 0.33, q = 0)$ and 'ultimate' $(p \simeq 0.55, q = 1)$ scalings is obtained from

$$Nu_{\mathrm{X}} \sim Ra_{\mathrm{X}}^{0.33} \sim (\ell/H)\,Ra_{\mathrm{X}}^{0.55}\,. \tag{6}$$

The two expression on the right can be solved for Ra_{X} such that substitution yields a transformation of Nu and Ra in terms of ℓ/H. The same transformation collapses ODT and reference results equally well onto the same master curve.

In order to consolidate the regime transition, extreme excursions in the temperature difference fluctuations, $\Delta T'(t) = \Delta T(t) - \langle \Delta T \rangle$, may adversely effect convergence. This places a burden on ODT simulations since long simulation times are needed for every realization in an ensemble to assure sufficient sampling of the state space attractor. This yields two potential problems. First, according to the definitions in (4), the Nusselt number exhibits an inverse proportionality on the temperature difference. Taking the instantaneous values suggests $Nu^*(t) \sim \Delta T^{-1}(t)$, so that $\langle \Delta T \rangle$ is a biased estimator for the average $Nu = \langle Nu^*(t) \rangle$. Second, because of the established ultimate scaling $Nu \sim (\ell/H)\,Ra^p$ (see Fig. 7), the unbiased estimator $\hat{p}$ for power-law scaling is given by inverse log-based statistics on the instantaneous temperature difference, that is,

$$\hat{p} = \left\langle \frac{1}{\ln\left[\Delta T^*(t)/\Delta T_0\right]} \right\rangle\,, \tag{7}$$

where ΔT_0 is a proportionality factor from $Ra = \langle \Delta T \rangle / \Delta T_0$.

Figure 8 shows the comparison of p obtained via the biased and unbiased estimator, respectively, selecting at least four consecutive data points ℓ/H for every prescribed Ra_P from the central transition region in Fig. 7. the simulated scaling exponent p is robust since independent of the selected estimator. This suggests that sufficiently long statistical sampling has been performed, which establishes the classical regime with $p \simeq 0.3$ and the 'ultimate' regime with $p \gtrsim 0.5$, which is overall in good agreement with available reference data.

Detailed Statistics of Turbulent Length Scales

Figure 9 shows the joint probability density function of the turbulent length scale λ and the lower edge location z_0 of the turbulent mappings defined in Fig. 2 above in double-logarithmic scaling. Both cases are from a highly turbulent regime with a broad scale range, offering comparable probability density magnitudes. The bright region on the right represents small-scale bulk turbulence with overturning fluid motions being farther away from the lower domain boundary than their size. The diagonal from the lower left to the upper right represents wall-attached turbulence. The upper left

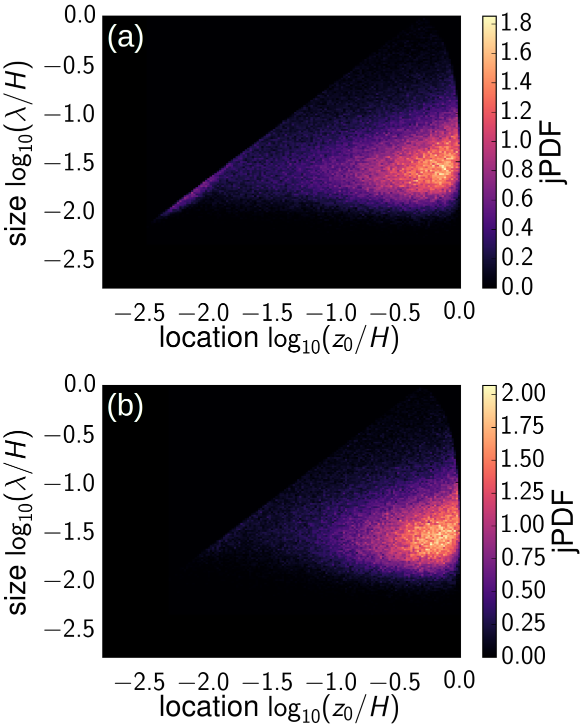

Figure 9. Joint probability density function (jPDF) of the stochastically sampled mapping events of an ODT simulation. $Ra_P = 10^{13}$, $\ell/H = 0.0015$, classical regime, (a). $Ra_P = 10^{13}$, $\ell/H = 0.0960$, 'ultimate' regime (b).

triangle is geometrically forbidden. Comparing the two results, it is apparent that the case from the classical regime exhibits small-scale wall-attached turbulence (bright line on the lower left side of the diagonal) that is absent in the case from the 'ultimate' regime, which is by analogy compatible with Grossmann & Lohse (2000), with the exception that the thermal boundary layer is not contributing to the overall heat flux while affecting the near-wall fluid temperature at the insulated no-slip wall that is used in the analysis.

CONCLUSION

Effects of the forcing length scale on the turbulent transition between diffusion and mixing-length dominated regimes in radiatively driven convection have been investigated with one-dimensional turbulence. The model has been applied standalone to a source-sink-type vertical convection system that is bounded by perfectly insulated no-slip walls, in which the conductive heat-escape bottleneck of isothermal walls can be bypassed. The model robustly predicts the turbulent transition for various parameter combinations in the asymmetrically forced setup reproducing and extending reference experiments. An ultimate regime with slightly 'super-ultimate' effective scaling $Nu \sim Ra^p$ with $p = 0.55 \gtrsim 1/2$ for large forcing length scales on the order of the confinement length scale. The result is robust against the statistical estimator used so that convergence issues can be largely ruled out. This suggests that $p > 1/2$ is a transitional effect that occurs when the internal heat source is affected by the confinement. Forthcoming research addresses turbulence statistics and a symmetric heating configuration to bridge the gap to canonical Rayleigh–Bénard convection to address and benefit from rigorous bounds on heat transport in transitional regimes.

ACKNOWLEDGMENT

This research is supported by the German Federal Government, the Federal Ministry of Research, Technology and Space, and the State of Brandenburg within the framework of the joint project "EIZ: Energie-Innovationszentrum" (project numbers 85056897 and 03SF0693A) with funds from the Structural Development Act for coal-mining regions.

REFERENCES

Arslan, A., Fantuzzi, G., Craske, J. & Wynn, A. 2021 Bounds on heat transport for convection driven by internal heating. *J. Fluid Mech.* **919**, A15.

Bouillaut, V., Flesselles, B., Miquel, B., Aumaître, S. & Gallet, B. 2022 Velocity-informed upper bounds on the convective heat transport induced by internal heat sources and sinks. *Phil. Trans. R. Soc. A* **380** (2225), 20210034.

Bouillaut, V., Lepot, S., Aumaître, S. & Gallet, B. 2019 Transition to the ultimate regime in a radiatively driven convection experiment. *J. Fluid Mech.* **861**, R5.

Chandrakar, K. K., Cantrell, W., Krueger, S., Shaw, R. A. & Wunsch, S. 2019 Supersaturation fluctuations in moist turbulent Rayleigh–Bénard convection: a two-scalar transport problem. *J. Fluid Mech.* **884**, A19.

Chillà, F. & Schumacher, J. 2012 New perspectives in turbulent Rayleigh–Bénard convection. *Eur. Phys. J. E* **35**, 58.

Goluskin, D. 2016 *Internally Heated Convection and Rayleigh–Bénard Convection*, 1st edn. *SpringerBriefs in Applied Sciences and Technology*. Cham: Springer.

Gonzalez-Juez, E. D., Kerstein, A. R. & Lignell, D. O. 2013 Reactive Rayleigh–Taylor turbulent mixing: a one-dimensional-turbulence study. *Geophys. Astro. Fluid Dyn.* **107**, 506–525.

Grossmann, S. & Lohse, D. 2000 Scaling in thermal convection: A unifying theory. *J. Fluid Mech.* **407**, 27–56.

Kazemi, S., Ostilla-Mónico, R. & Goluskin, D. 2022 Transition between boundary-limited scaling and mixing-length scaling of turbulent transport in internally heated convection. *Phys. Rev. Lett.* **129**, 024501.

Kerstein, A. R. 1999 One-dimensional turbulence: Model formulation and application to homogeneous turbulence, shear flows, and buoyant stratified flows. *J. Fluid Mech.* **392**, 277–334.

Kerstein, A. R., Ashurst, W. T., Wunsch, S. & Nilsen, V. 2001 One-dimensional turbulence: vector formulation and application to free shear flows. *J. Fluid Mech.* **447**, 85–109.

Klein, M. & Schmidt, H. 2019 Investigating Rayleigh–Bénard convection at low Prandtl numbers using one-dimensional turbulence modeling. In *Proc. 11th Int. Symp. Turb. Shear Flow Phen. (TSFP-11)*. Southampton, UK.

Kraichnan, R. H. 1962 Turbulent thermal convection at arbitrary Prandtl number. *Phys. Fluids* **5**, 1374.

Lepot, S., Aumaître, S. & Gallet, B. 2018 Radiative heating achieves the ultimate regime of thermal convection. *PNAS* **115** (36), 8937–8941.

Lignell, D. O., Kerstein, A. R., Sun, G. & Monson, E. I. 2013 Mesh adaption for efficient multiscale implementation of one-dimensional turbulence. *Theor. Comput. Fluid Dyn.* **27** (3), 273–295.

de Lozar, A. & Mellado, J. P. 2015 Mixing driven by radiative and evaporative cooling at the stratocumulus top. *J. Atmos. Sci.* **72** (12), 4681–4700.

Malkus, W. V. R. 1954 Discrete transitions in turbulent convection. *Proc. Royal Soc. Lond. A* **225**, 185–195.

Shraiman, B. I. & Siggia, E. D. 1990 Heat transport in high-

Rayleigh-number convection. *Phys. Rev. A* **42**, 3650–3653.

Spiegel, E. A. 1963 A generalization of the mixing-length theory of thermal convection. *Asrophys. J.* **138**, 216–225.

Wang, Q., Lohse, D. & Shishkina, O. 2021 Scaling in internally heated convection: A unifying theory. *Geophys. Res. Lett.* **48** (4), e2020GL091198.

Wunsch, S. & Kerstein, A. R. 2005 A stochastic model for high-Rayleigh-number convection. *J. Fluid Mech.* **528**, 173–205.